Wear xxx (xxxx) xxx

Contents lists available at ScienceDirect

Wear

journal homepage: www.elsevier.com/locate/wear

Cracking behavior of wear resistant TiAlCrSiN coated cemented carbide compounds

K. Bobzin, C. Kalscheuer, M. Tayyab *

Surface Engineering Institute, RWTH Aachen University, Kackertstraße 15, 52072, Aachen, Germany

ARTICLE INFO

Keywords:
PVD
nanocomposite
Crack resistance
Nanoindentation

ABSTRACT

Due to their high hardness and thermal stability, nanocomposite TiAlCrSiN coatings represent a current trend in physical vapor deposition (PVD)-based wear resistant tool coatings. As PVD-coated tools are subjected to high loads during application, it is imperative to investigate their cracking behavior in order to improve wear resistance. Here, coating thickness, coating architecture and deformation behavior of coated compound may affect the service life of the coated tool. Hence, current study compared cracking behavior of monolayer TiAlCrSiN and bilayer TiAlCrSiON/TiAlCrSiN coatings with varying coating thicknesses for cemented carbide-based tool applications. Monolayer TiAlCrSiN and bilayer TiAlCrSiON/TiAlCrSiN, each with thickness s = ~1.9 µm and s = ~3.5 µm were deposited on cemented carbide substrates and characterized. The coated compounds as well as uncoated substrates were subjected to quasi-static nanoindentations with F = 750 mN, F = 1000 mN and F = 1250 mN and nanoscratches with F = 300 mN, F = 500 mN and F = 1000 mN. A conical-shaped diamond indenter tip was used for this purpose. The indent imprints were analyzed for surface cracks using scanning electron microscopy. Nanoscratches were additionally analyzed in cross-section and their indentation depth was measured with confocal laser scanning microscopy. The oxynitride top layer led to a reduced indentation hardness H_{IT} for bilayer variant. For both coating architectures, an increase in coating thickness did not significantly affect H_{IT}. However, with the increase in coating thickness the indentation depth reduced and the crack resistance of the coated compounds improved under considered loading conditions. Moreover, the bilayer variant showed higher resistance against surface cracks under sliding load. Compared to the uncoated substrate, the coated compounds showed lower indentation depth and increased crack resistance. The study contributes to fundamental understanding of deformation and cracking behavior of cemented carbide tools with nanocomposite coatings for wear resistance improvement.

1. Introduction

For productivity improvement of manufacturing processes, tool service life plays an important role. Physical vapor deposition (PVD) nitride hard coatings are widely used in the industry to improve wear resistance of cutting and forming tools. However, with ongoing development of new difficult to process materials, the manufacturing processes and the corresponding stress collectives on tools are becoming increasingly challenging. This has led to an increased demand for advanced PVD nanocomposite wear resistant coatings in addition to commonly used polycrystalline TiN, TiAlN or CrAlN systems. Nanocomposite coatings may deliver superior hardness and crack resistance for challenging tooling applications [1,2]. TiAlCrSiN represents one of the advanced nanocomposite coating systems, which offers the possibility to combine the advantages of Al, Cr and Si addition to TiN in a single coating system. Compared to binary TiN, incorporation of Al and Cr may improve the oxidation resistance and hardness of the resulting coatings [3]. Si addition in polycrystalline TiN or TiAlN coating systems leads to formation of amorphous phase and restricts the grain growth [1]. This results in a nanocomposite structure, where crystalline (Ti,Al,Cr)N nanograins are surrounded by an amorphous Si_3N_4-matrix. Previous investigations have shown promising application behavior of TiAlCrSiN nanocomposites as wear resistant tool coatings for challenging cutting applications [4,5]. A further addition of oxygen may also reduce the adhesion tendency of the steel workpiece material to TiAlCrSiON coated cutting tool [6]. However, depending on the oxygen

This article is part of a special issue entitled: WOM2025 published in Wear.

* Corresponding author.
E-mail address: tayyab@iot.rwth-aachen.de (M. Tayyab).

https://doi.org/10.1016/j.wear.2025.205810
Received 6 September 2024; Received in revised form 9 December 2024; Accepted 13 December 2024
Available online 28 January 2025

content, an increased amorphous content and decreased hardness of monolayer oxynitride coatings may reduce the abrasive wear resistance of the tool [7]. A bilayer architecture with nitride interlayer and an oxynitride top layer offers one of the ways to explore the advantageous potential of oxygen incorporation in nitride hard coatings.

As protective tool coatings for challenging manufacturing process, coating thickness, architecture as well as deformation and cracking behavior of the coated compound can affect the tool performance [8]. Several fundamental level investigations have focused on cracking behavior of PVD-coated compounds to understand the underlying deformation and failure mechanisms in correlation with coating and substrate properties. For instance, in Ref. [9], the deformation mechanisms of columnar TiN coatings on Si substrate were investigated under quasi-static normal load. Here, column inclination and grain boundary sliding were established as main coating deformation mechanisms. In Ref. [10], the coating deformation and crack mechanisms were understood under sliding normal load for columnar CrAlN coatings on X46Cr13 steel substrates. The effect of coating architecture on crack initiation and propagation in Cr/CrN multilayer coatings using nanoindentation was studied in Ref. [11]. The cracks mainly initiated in hard CrN layers while relatively ductile Cr layers were able to sustain large plastic strains. The cracking behavior of TiAlN monolayer and Ti/TiAlN multilayer coatings on Ti–6Al–4V substrates under sliding normal load was studied in Ref. [12]. Compounds with monolayer variant showed lower load bearing capacity and crack resistance. The ductile Ti layer enhanced the toughness of the multilayer coatings. The effect of substrate deformation behavior on crack resistance of TiAlN/X153CrMoV12 tool steel compounds for tooling applications was studied in Ref. [13]. Specifically placed indents on large carbide inclusions and martensite matrix locations in the coated substrate were analyzed for coating cracks. The indents on martensite matrix locations showed higher indentation and depth and inter-columnar shear cracking in the coating. The influence of coating thickness in terms of deformation behavior and damage initiation in CrAlN/HS6-5-2C compounds under cyclic impact loading was addressed in Ref. [14]. In case of cemented carbide substrates for cutting tool applications, the cracking behavior of Ti, Al, Cr and Zr based multilayer nitride coatings was studied in Refs. [15,16] to adjust the coating properties for higher fracture toughness and tool life. The fundamental investigations, in case of TiAlCrSiN nanocomposite coatings for cemented carbide tools, are missing in literature. Hence, current study focuses on cracking behavior of monolayer TiAlCrSiN and bilayer TiAlCrSiON/TiAlCrSiN coatings with varying coating thicknesses for cemented carbide-based tooling applications. A combination of nanoindentation and electron microscopy is used to understand the effect of coating thickness and architecture on cracking behavior of coated compounds under quasi-static and sliding normal loading conditions.

2. Experimental methods

2.1. Coating deposition

Two coating architectures, monolayer TiAlCrSiN and bilayer TiAlCrSiON/TiAlCrSiN, each with intended coating thickness s = ~1.9 µm and s = ~3.5 µm, were deposited on cemented carbide inserts SNUN 120412, ISO code K20-K40 and grade CTS18D, CERATIZIT Luxembourg S.á.r.l, Mamer, Luxembourg. The monolayer architecture consisted of a single TiAlCrSiN layer, whereas bilayer coating architecture comprised of TiAlCrSiN interlayer and an oxynitride TiAlCrSiON top layer. For coating deposition, an industrial PVD unit CC800/9 HPPMS, CemeCon AG, Wuerseln, Germany, was used. In total four coating variants were produced using same target configuration, see Fig. 1. High power pulse magnetron sputtering (HPPMS) cathodes were operated with TiAl48 and TiAl20 targets. The TiAl48 und TiAl20 targets consisted of 40 and 20 Al plugs, respectively. Pure Si and Cr targets were installed on direct current magnetron sputtering (dcMS) cathodes. During the coating

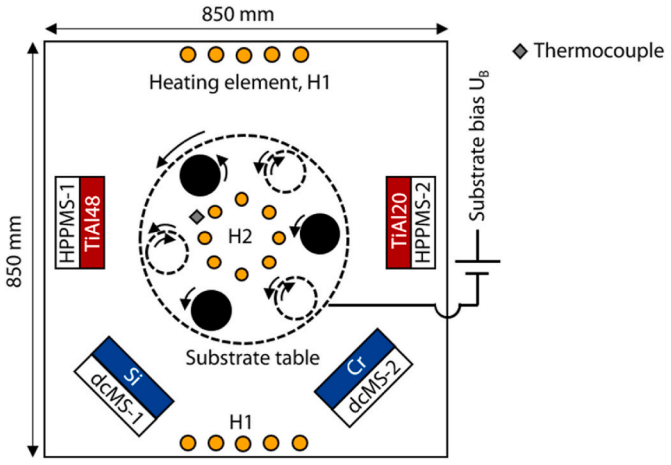

Fig. 1. Schematic representation of coating chamber of industrial coating unit CC800/9 HPPMS.

deposition, the substrate samples were subjected to a three-fold rotation with table speed $n_{Table} = 2.5\ min^{-1}$. In order to measure the temperature inside the coating chamber, a K-Type thermocouple was used. The approximate location of thermocouple inside the coating chamber is marked in Fig. 1.

The process parameters for deposition of the investigated coatings are shown in Table 1. The coating processes were run at least three times to ensure process repeatability. The coatings were intended to have high content of the target materials operated with the HPPMS cathodes. Hence, HPPMS cathodes were operated at significantly higher power compared to dcMS cathodes. In order to improve the adhesion between the coating and substrate, all four coating processes were designed to have a TiAlCrN bond layer. The influence of bond layer thickness on subsequent investigations was minimized by keeping a constant bond layer coating time for all investigated coating variants. The coating process of monolayer TiAlCrSiN was used as the basis for bilayer architecture, which means the process parameters until the deposition of TiAlCrSiON were same for the two coating architectures, see Table 1. In

Table 1
Process parameters of investigated coatings.

Coating process	Monolayer TiACrSiN	Bilayer TiAlCrSiON/TiAlCrSiN
Sample ID/-	5067[a] & 5071[b]	5072[a] & 5068[b]
Pressure p/mPa	520	520
Argon flow $Q(Ar)$/sccm	200	200
Nitrogen flow $Q(N_2)$/sccm	Pressure controlled	Pressure controlled
Oxygen flow $Q(O_2)$/sccm	–	18[c]
Heating power on sides P_{H1}/kW	8	8
Heating power in middle P_{H2}/kW	4	4
Maximum coating temperature T_{max}/°C	590	590
Substrate bias U_B/V	−80	−80
Average power of HPPMS cathodes P_{HPPMS}/kW	7	7
Power dcMS-1 $P_{dcMS\text{-}1}$/kW	0.6	0.6/1.0[c]
Power dcMS-2 $P_{dcMS\text{-}2}$/kW	0.3	0.3/0.7[c]
Pulse frequency f/Hz	2000	2000
Pulse duration t_{on}/µs	60	60
Coating time TiAlCrN Bond layer $t_{TiAlCrN}$/s	5400	5400
Coating time TiAlCrSiN $t_{TiAlCrSiN}$/s	8300[a] & 16,000[b]	5400[a] & 10,800[b]
Coating time TiAlCrSiON $t_{TiAlCrSiON}$/s	–	2700[a] & 4500[b]

[a] Thin coating.
[b] Thick coating.
[c] During deposition of TiAlCrSiON.

Table 2
Coating thickness s, area average roughness Sa, chemical composition, indentation hardness H_{IT}, indentation modulus E_{IT} and adhesion strength class HF of investigated monolayer TiAlCrSiN and bilayer TiAlCrSiON/TiAlCrSiN thin as well as thick coatings.

Coating architecture	Monolayer-Thin	Bilayer-Thin	Monolayer-Thick	Bilayer-Thick
s/µm	1.9	2.0	3.4	3.7
Sa/µm	0.05	0.05	0.1	0.08
Ti/at.%	17	15	17	15
Al/at.%	26	21	26	21
Cr/at. %	2	4	2	4
Si/at. %	2	3	2	3
O/at. %	<0.5	22	<0.5	22
N/at. %	53	37	53	37
H_{IT}/GPa	31.7 ± 1.5	25.7 ± 2.5	30.5 ± 2.3	25.0 ± 2.1
E_{IT}/GPa	390.6 ± 15.5	345.9 ± 26.6	353.0 ± 20.6	327.8 ± 24.0
HF/-	1	1	1	1

case of bilayer architecture, oxygen with a flowrate $Q(O_2)$ = 18 sccm was introduced after deposition of TiAlCrSiN interlayer. As mentioned in Ref. [6], the introduction of oxygen may lead to poisoning of dcMS operated Si and Cr targets, resulting in reduced Si and Cr incorporation in oxynitride top layer. In order to minimize the influence of target poisoning on Si and Cr content of oxynitride layer, the power of dcMS-1 and dcMS-2 was increased during deposition of TiAlCrSiON top layer, see Table 1. The coating time for TiAlCrSiN interlayer and TiAlCrSiON top layer was adjusted to achieve a comparable coating thickness to monolayer TiAlCrSiN. Moreover, for variation of overall coating thickness, namely thin and thick variants of each coating architecture, the coating times were adjusted, see Table 1. The coating times for TiAlCrSiN and TiAlCrSiON deposition were almost doubled for thick coatings as compared to their thin variants. Remaining process parameters for thick variants of monolayer TiAlCrSiN and bilayer TiAlCrSiON/TiAlCrSiN were identical to their corresponding thin variants (see Table 2).

2.2. Coating and compound characterization

Fracture cross-sections of coated samples were examined by scanning electron microscopy (SEM) to analyze coating morphology and to determine coating thickness. For this purpose, Zeiss DSM 982 Gemini, Carl Zeiss AG, Oberkochen, Germany, was used. Electron probe microanalysis (EPMA) was carried out to determine the chemical composition of the coatings. For this purpose, JEOL JXA-8530F from JEOL Ltd., Tokyo, Japan, was used. SEM and EPMA investigations were carried out at Central Facility for Electron Microscopy (GFE), RWTH Aachen University, Aachen, Germany. Area average roughness Sa of the coated compounds was measured by confocal laser scanning microscope (CLSM), Keyence VK-X210, Tokyo, Japan. In order to determine the indentation hardness H_{IT} and indentation modulus E_{IT} of the coatings, nanoindentation measurements were carried out using a calibrated TriboIndenter TI 950, Bruker Corporation, Billerica, Massachusetts, USA. A Berkovich shaped diamond indenter tip with nominal radius r ≈ 150 nm was used for this purpose. For each coating variant, 50 measurements with maximum indentation force F = 8 mN were carried out as per ISO 14577–4:2016. Indentation hardness H_{IT} and indentation modulus E_{IT} were calculated from measured force-displacement data as per the method suggested by Oliver and Pharr [17]. For calculations, Poisson's ratio ν = 0.25 for nitride coatings was assumed [18,19]. The adhesion between the coating and the cemented carbide substrate was measured as per DIN 4856 Rockwell C indentation method. The coated samples were subjected to a normal force F ≈ 588.4 N using a diamond indenter with cone angle α = 120° installed on HP100 Rockwell tester, KNUTH Machine Tools GmbH, Wasbek, Germany. In order to determine the adhesion strength class (HF), the Rockwell indents were analyzed by CLSM.

2.3. High load nanoindentations and nanoscratches

The cracking behavior of uncoated cemented carbide as well as coated compounds was investigated under two loading conditions, quasi-static normal load and sliding normal load. For quasi-static normal loading, nanoindentations were carried out with a maximum normal force F = 750 mN, F = 1000 mN and F = 1250 mN. For this purpose, a conical shaped diamond indenter with nominal cone angle α = 60° and nominal radius r = 10 µm was installed on Nanoindenter UNAT, ASMEC GmbH, Dresden, Germany. The load function consisted of three segments with their corresponding time durations, namely loading with $t_{loading}$ = 10 s, hold with t_{hold} = 3 s and unloading with $t_{unloading}$ = 10 s. For each sample variant and maximum indentation force F, three measurements were carried out. The deformation behavior of the uncoated cemented carbide as well as coated compounds was characterized by examining the force-displacement curves from measurements. Here, maximum indentation depth h_{max}, permanent indentation depth h_p, elastic work percentage η_{elast} and plastic work percentage η_{plast} were determined. Permanent indentation depth h_p represents the remaining depth of the indent after unloading and elastic recovery of the sample. The elastic η_{elast} and plastic η_{plast} work percentages represent percentual contributions of elastic reverse deformation work W_{elast} and plastic deformation work W_{plast}, respectively, to the total work W_t during indentation. W_{plast} represents the area between loading and unloading curve, while W_{elast} denotes area below the unloading curve. The indents at considered normal loads were analyzed for surface cracks using SEM.

In order to investigate the cracking behavior under sliding normal load, nanoscratch tests on uncoated cemented carbide and coated compounds were carried out. Here, the same equipment and conical indenter was used, as previously mentioned for quasi-static loading condition. Nanoscratch tests were carried out with normal force F = 300 mN, F = 500 mN and F = 1000 mN and sliding velocity v_s = 10 µm/s. For each sample variant and normal force, three nanoscratches were carried out. The deformation behavior of the samples under sliding normal load was characterized by determination of permanent scratch depth $h_{p,s}$ with CLSM and analysis of fracture cross-sections of scratch tracks with SEM. Moreover, the scratch tracks were analyzed for surface cracks using SEM. The crack initiation and propagation in coating cross-section was studied through a combination of focused ion beam (FIB) and scanning transmission electron microscopy (STEM). Here, three FIB lamellae from selected coated compounds were cross-sectionally cut to the scratch track using PFIB Helios 5, Thermo Fischer Scientific, Eindhoven, Netherlands, as exemplarily shown in Fig. 2. The FIB lamellae were analyzed with STEM using FEI Tecnai G^2 F20 S-TWIN, Thermo Fischer Scientific, Eindhoven, Netherlands. The FIB preparations as well as SEM and STEM investigations were carried out at GFE.

3. Results and discussion

3.1. Coating and compound properties

Coating thickness, chemical composition of the top layer, area average roughness Sa, indentation hardness H_{IT}, indentation modulus E_{IT} and adhesion strength class HF of the thin as well as thick coating variants are mentioned in Table 1. For bilayer coating architecture, the chemical composition of TiAlCrSiN interlayer is similar to monolayer TiAlCrSiN. Moreover, the thin coating variants also have a similar chemical composition to their corresponding thick variants.

For TiAlCrSiON top layer, incorporation of oxygen mainly came at the expense of nitrogen along with minor contributions from Ti and Al. As compared to TiAlCrSiN, the oxynitride TiAlCrSiON top layer showed an increased non-metallic content in terms of atomic percentage contributions of N and O. Accordingly, the bilayer variants exhibited a reduced indentation hardness H_{IT} and indentation modulus E_{IT}

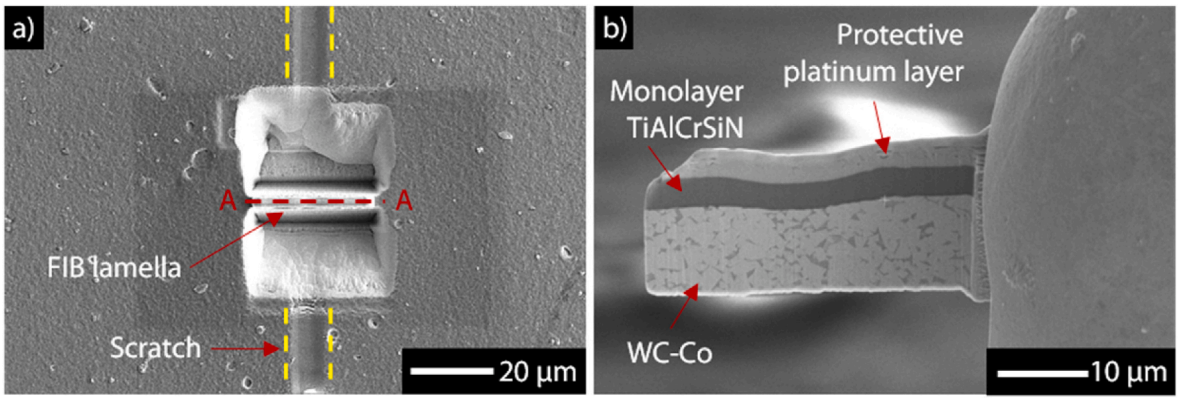

Fig. 2. (a) Location and orientation of FIB lamella along with (b) SEM image of the prepared lamella from cross-section A-A.

compared to the monolayer variant. This may be attributed to the higher amorphous content of the oxynitride TiAlCrSiON. As mentioned in Refs. [2,5], Si and O incorporation in nitride hard coatings may lead to formation of amorphous phases in the coating. The indentation hardness H_{IT} of the thin coatings is comparable to their corresponding thick variants. However, an increase in coating thickness resulted in a slight decrease in indentation modulus E_{IT} of the monolayer TiAlCrSiN and bilayer TiAlCrSiON. Fracture cross-sections of the coatings are shown in Fig. 3. All coatings exhibit similar cauli-flower like morphology resulting from large clusters of fine vertical columns. The thick coatings comprise of lengthier columns as compared to their thin variants.

3.2. *Cracking behavior under quasi-static normal loading*

Fig. 4 summarizes the results from quasi-static nanoindentations of uncoated cemented carbide and coated compounds regarding their deformation and cracking behavior at varying loads. Fig. 4a) represents the average maximum indentation depth h_{max} as a sum of h_p and h_e plus the average total work of indentation W_t. Permanent indentation depth h_p denotes the remaining depth of the indent after unloading, whereas h_e characterizes the difference in h_{max} and h_p resulting from elastic recovery of the material. W_t represents the area under the loading segment of the force-displacement indentation curve. Fig. 4b) displays the average percentual contributions from plastic work percentage η_{plast} and elastic recovery work η_{elast} to the total work W_t during indentation. It is important to note here that the work percentages are calculated from the measured force-displacement data during indentation. Any contributions from crack initiation and propagation in material to the total energy dissipation during indentation is not separately considered. As apparent from the results, the coated compounds exhibit a higher resistance against surface cracks as compared to the uncoated cemented carbide. This could be attributed to the higher load bearing capacity or resilience of the nitride hard coatings as indirectly characterized by W_t, η_{plast} and η_{elast}. The coated compounds consistently showed reduced total indentation work W_t, plastic work percentage η_{plast} and higher elastic recovery in terms of η_{elast} as compared to uncoated cemented

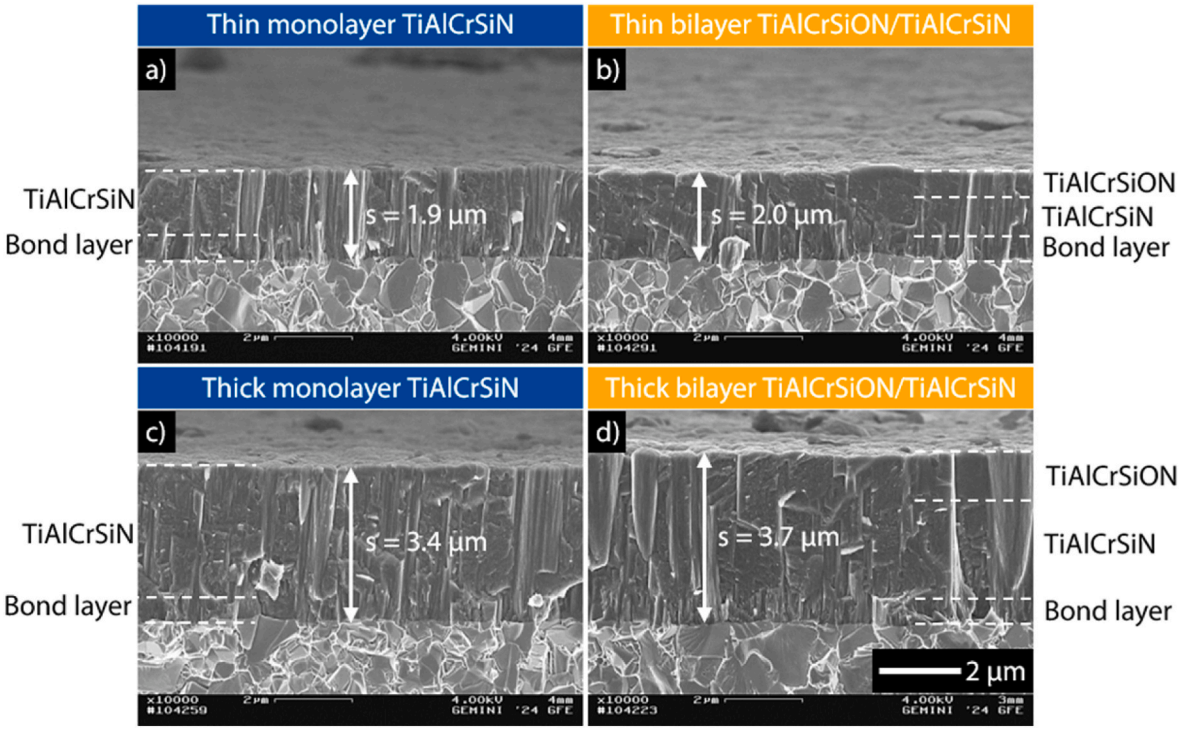

Fig. 3. SEM images of fracture cross-sections of (a) thin monolayer TiAlCrSiN, (b) thin bilayer TiAlCrSiON/TiAlCrSiN, (c) thick monolayer TiAlCrSiN and (d) thick bilayer TiAlCrSiON/TiAlCrSiN.

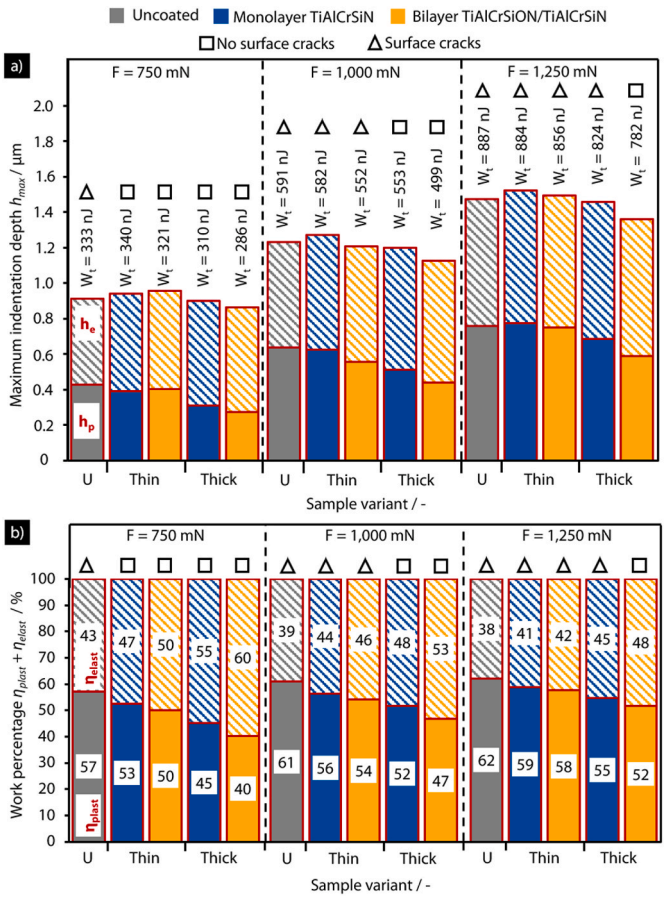

Fig. 4. (a) Maximum indentation depth h_{max}, total indentation work W_t, (b) plastic work percentage η_{plast} and elastic work percentage η_{elast} of uncoated cemented carbides and coated compounds at maximum indentation force F = 750 mN, F = 1000 mN and F = 1250 mN.

carbide. Among the coated compounds, an increase in coating thickness seems to improve the resistance of the coated compounds against surface cracks. An increase in coating thickness resulted in reduced h_{max}, h_p, W_t and η_{plast} for the coated compounds. This points towards increased load bearing capacity of the thick coatings compared to their thin variants. In terms of coating architecture, the bilayer architecture showed a slightly reduced h_p, W_t and η_{plast} for thin and thick variants compared to the corresponding monolayer coatings. However, any difference in resistance against surface cracks became apparent only at F = 1250 mN in case of thick coatings. This points towards the promising potential of bilayer architecture with oxynitride top layer to improve the resistance of the coated compound against surface cracks. In present case, the plastic work percentage η_{plast} seems to be an essential parameter for resistance of coated compounds against surface cracks under quasi-static loading. Irrespective of the coating thickness and indentation force, the coated variants with $\eta_{plast} \leq 53$ % showed no surface cracks around the indents. The plastic work percentage η_{plast}, calculated from the nanoindentation data, could be helpful in studying the surface crack resistance of the compounds. As observed in present case, $\eta_{plast} \leq 53$ % appears to be the deformation limit of the coated compounds above which the surface cracks appear. Moreover, depending on the coating architecture and thickness, the n_{plast} limit for surface cracks was reached at different indentation forces for the considered compounds. Hence, n_{plast} may also be helpful in comparing the crack resistance of different coated variants. However, it is important to note that the n_{plast} limit observed in current study may not be the same for other coating and substrate material combinations and used indenter geometries.

Fig. 5 exemplarily illustrates the surface cracks for uncoated cemented carbide as well as coated compounds with thin monolayer TiAlCrSiN and thin bilayer TiAlCrSiON/TiAlCrSiN at F = 1250 mN. A comparable trend in terms of surface crack locations, when present, was observed for other combinations of indentation forces and sample variants. In Fig. 5a), c) and 5e) approximate area of the indent is marked with yellow circle whereas red arrows point out the locations of surface cracks. One of the surface crack locations as marked by red box is shown in an enlarged view in corresponding Fig. 5b), d) and 5f). The scratches visible on the surface of uncoated cemented carbide are because of the sample preparation as the substrates were polished before coating. The quasi-static nanoindentations on uncoated cemented carbide were carried out in initial substrate condition before coating. The surface cracks, in case of uncoated cemented carbide, were observed inside as well as in the boundary region of the indent. The boundary region of the indent exhibited circumferential and radial surface cracks, see Fig. 5b). For coated compounds, surface cracks were concentrated in boundary region of the indents. Moreover, only radial surface cracks, proceeding outwards from the boundary region, were observed, see Fig. 5d) and f). The path of radial surface cracks appeared to be mostly limited along the boundaries of large column clusters or through the clusters along the boundaries of individual fine columns. Moreover, the radial cracks, in case of coated compounds, were lengthier as compared to the uncoated substrate. Inside the indent area on coated compounds, no large surface cracks were observed. The large column clusters seem to be pushed down and pressed against each other resulting in surface flattening inside the indent area. This, along with the additional compressive residual stresses due to the deformation, may have prevented any initiation of surface cracks inside the indent area. As the current investigation focused on large surface cracks, the possibility of smaller cracks in submicron range in coating cross-section, resulting from shear sliding between columnar grains inside the indent area, cannot be ruled out.

3.3. Cracking behavior under sliding normal load

Fig. 6 summarizes the results from nanoscratch tests on uncoated cemented carbide and coated compounds regarding their deformation and cracking behavior at varying normal loads. The coated compounds exhibited average lower permanent scratch depth $h_{p,s}$ and higher resistance against surface cracks as compared to the uncoated cemented carbide. Among the coated compounds, a higher coating thickness positively influenced the load bearing capacity of the coated compound, as the permanent scratch depth $h_{p,s}$ decreased and the resistance against surface cracks increased. The thick coatings showed on average $\Delta h_{p,s} = (100 \pm 20)$ nm lower permanent scratch depth compared to their corresponding thin variants. Moreover, the bilayer coating architecture seems to contribute towards an increased resistance of the coated compound against surface cracks under sliding load. At F = 500 mN, the variant with thin bilayer TiAlCrSiON/TiAlCrSiN showed higher resistance against surface cracks compared to the variant with thin monolayer TiAlCrSiN. The same was true at F = 1000 mN for coated compounds with thick coatings.

In order to understand the coating and substrate deformation under sliding normal load, Fig. 7 exemplarily shows the fracture cross-sections and representative depth profiles of nanoscratches at F = 1000 mN. As compared to coated compounds, the uncoated cemented carbide underwent increased permanent deformation characterized by permanent scratch depth $h_{p,s}$. This resulted in significant bulging of the material around the shoulders of scratch track, see Fig. 7a). The outward protrusion of the material around scratch shoulders reduced significantly for coated compounds. This points towards increased load bearing capacity of the coated compounds. Moreover, the load bearing capacity of the coating increased with the coating thickness. At F = 1000 mN, the coated compounds with thin coatings, as compared to the variants with thick coatings, exhibited higher $h_{p,s}$ and material bulging around scratch shoulders along with slight permanent deformation of cemented carbide substrate, see Fig. 7b) and c). In case of thick coatings, the permanent

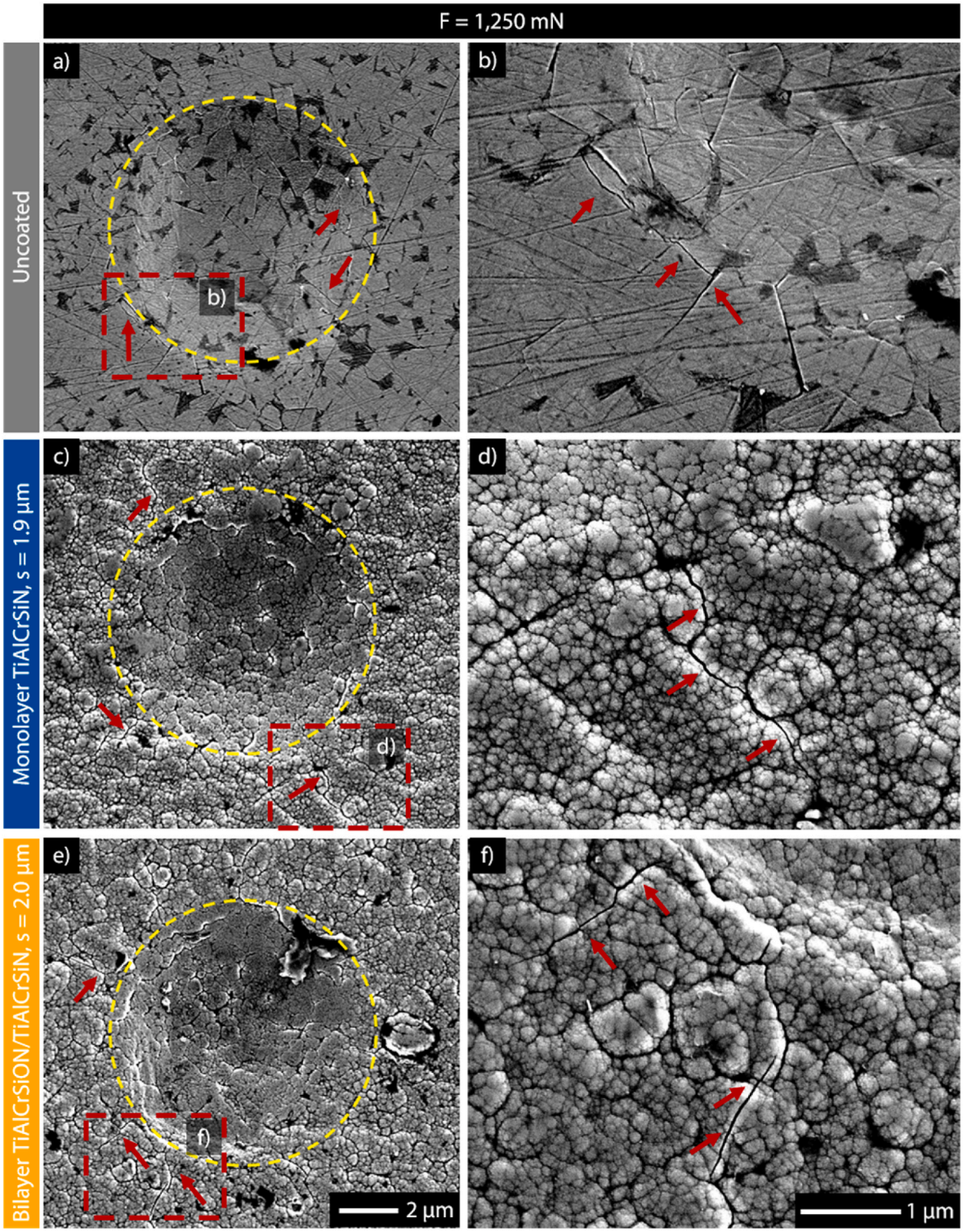

Fig. 5. Indent imprints and surface cracks for (a–b) uncoated cemented carbide, (c–d) coated compound with thin monolayer TiAlCrSiN and (e–f) coated compound with thin bilayer TiAlCrSiON/TiAlCrSiN subjected to maximum indentation force F = 1250 mN.

deformation was largely limited to the coating, see Fig. 7d) and e). This explains the increased surface crack resistance of the coated compounds with higher coating thickness. As compared to F = 1000 mN, the coated compounds at F = 500 mN exhibited reduced material bulging around scratch shoulders with permanent deformation largely concentrated in the coating. Other than that, a similar trend in terms of the coating thickness effect, as discussed for F = 1000 mN, was observed at F = 500 mN.

Fig. 8 exemplarily illustrates the surface cracks for uncoated cemented carbide as well as coated compounds with thin monolayer TiAlCrSiN and thin bilayer TiAlCrSiON/TiAlCrSiN at F = 1000 mN and additionally at F = 500 mN for thin bilayer TiAlCrSiON/TiAlCrSiN variant. A comparable trend in terms of surface cracks locations, when present, was observed for other combinations of normal forces and sample variants. The cracks for uncoated cemented carbide as well as coated compounds were mostly limited inside the scratch track. As

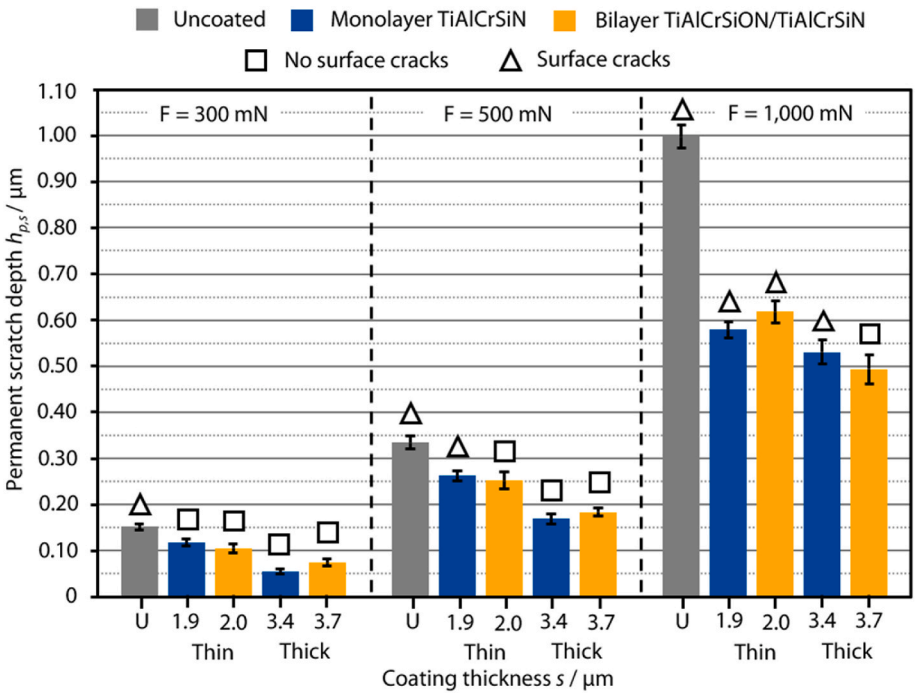

Fig. 6. Permanent scratch depth $h_{p,s}$ and surface crack analysis results for uncoated cemented carbide and coated compounds from nanoscratch tests with normal force F = 300 mN, F = 500 mN and F = 1000 mN.

known from scratch tests, the surface cracks originated from the central zone of the scratch track, where highest pressure is applied from the indenter. The material protrusion around scratch shoulders, in case of uncoated cemented carbide, can be seen in Fig. 8a). For coated compounds, no adhesive or cohesive failure of the coatings was observed for the considered loading conditions. However, surface cracks in coatings were lengthier than the ones observed for uncoated cemented carbide. Additionally, for thin bilayer TiAlCrSiON/TiAlCrSiN at F = 1000 mN, the surface morphology inside the scratch track changed as the columnar structure and their boundaries were not distinguishable, see Fig. 8e) and f). The same was also true for the thick bilayer variant. A further iteration of nanoscratch tests with the same conditions showed similar results. This extreme flattening of the surface and non-visibility of columnar structure was not the case for the same coating at F = 500 mN, see Fig. 8g) and h). There could be two hypotheses, which can explain this effect. In first hypothesis, the thin reaction layer on the oxynitride top layer may have detached at high normal force and rubbed over the surface to cover the columnar morphology. The second hypothesis, proposed in Ref. [20], is based on presence of low melting phases in passive layer for an oxynitride coating. When subjected to severe pressing from the sliding indenter, these phases may undergo a short-time liquification and cover the boundaries of coating columns before solidification. However, further investigations are required to validate any of the two hypotheses.

The initiation and propagation of cracks in cross-section of selected scratches was analyzed through a combination of FIB and STEM. Fig. 9 exhibits the STEM dark field (DF) images of the FIB lamella from the scratch cross-section of coated compound with thin monolayer TiAlCrSiN at F = 1000 mN. The uneven platinum protective layer on top of TiAlCrSiN comes from the FIB lamella preparation. As apparent in Fig. 9a), the coating as well as substrate underwent a permanent deformation. In shoulder region of the scratch, a large crack was observed which ran through the TiAlCrSiN coating until the TiAlCrN bond layer, see Fig. 9b) and c). The crack seems to be a result of separation between two inclined column clusters, as marked by yellow dotted line in Fig. 9b. The interface region between TiAlCrSiN and TiAlCrN bond layer may act as barrier to crack propagation as the crack width reduced in the interface region, see Fig. 9c. Fig. 9d) and e) show an example of the crack, whose width reduced in the interface region between monolayer TiAlCrSiN and TiAlCrN bond layer and the crack path was limited to the start of TiAlCrN bond layer. Due to the deformation, the TiAlCrN bond layer also exhibited inclination of column clusters or individual columns as exemplarily marked by red dotted line in Fig. 9e). This column inclination may also initiate cracks within the TiAlCrN bond layer.

Fig. 10 additionally shows STEM bright field (BF) images from scratch shoulder region marked in Fig. 9a). In BF STEM mode the cracks are noticeable in white color.

As marked in Fig. 10a) and b), several micro- and macrocracks were observed in the region subjected to material bulging around scratch shoulder. The cracks seem to propagate along the boundaries of inclined columns of TiAlCrSiN and TiAlCrN. In addition to cracks, small areas with adhesive damage of the coating was observed in scratch shoulder region, see Fig. 10c) and d). The outward push from the material in central region of the scratch track combined with overall bending-shaped material deformation may subject the coating substrate interface at scratch shoulders to extreme tensile stresses resulting in initiation of adhesive failure i.e. debonding of the coating from the substrate.

Fig. 11 displays the STEM DF images of the FIB lamella from the scratch cross-section of coated compound with thick monolayer TiAlCrSiN at F = 1000 mN. The FIB lamella with thick monolayer TiAlCrSiN show an overall lower permanent deformation for coating and substrate as well as reduced crack formation as compared to the one with thin monolayer TiAlCrSiN. This confirms the increased load bearing capacity and crack resistance of the coated compounds with higher coating thickness. In shoulder and central region of the scratch track, thin microcracks largely limited to TiAlCrSiN were observed, see Fig. 11b), c) and 11d).

Fig. 12 shows the STEM DF images of the FIB lamella from the scratch cross-section of coated compound with thick bilayer TiAlCrSiON/TiAlCrSiN at F = 1000 mN. The increased amorphous content of the oxynitride top layer is evident by reduced texturing of the coating as compared to TiAlCrSiN interlayer or TiAlCrN bond layer. The nanolaminate structure, more evident within the TiAlCrSiON, represents

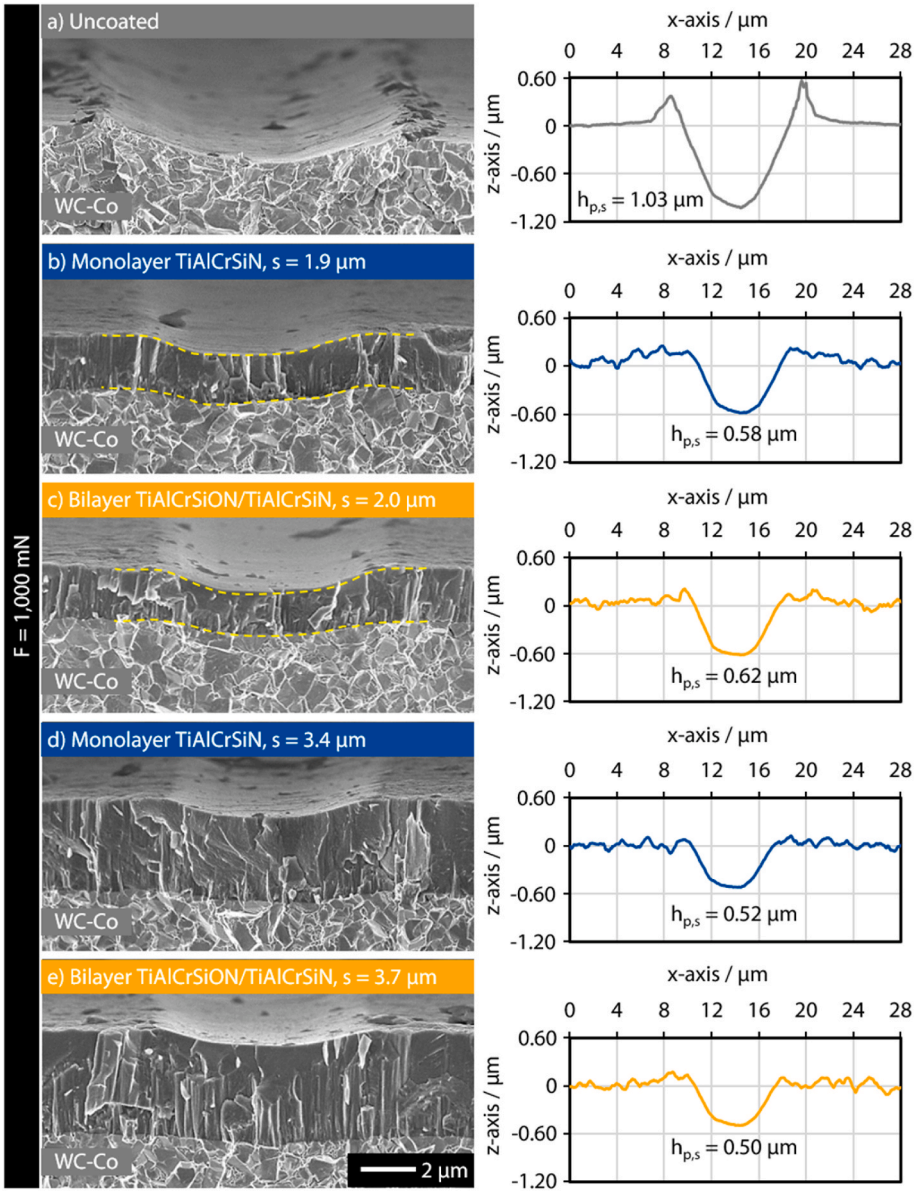

Fig. 7. SEM images of fracture cross-sections along with representative depth profiles of nanoscratches at F = 1000 mN for (a) uncoated cemented carbide and (b–e) coated compounds.

nanolayers of varying chemical composition resulting from the different target compositions used during the coating deposition, as common for the PVD coatings. Fig. 12a) and c) show thin microcracks observed in oxynitride top layer from scratch shoulder region. Here again, these cracks appear to propagate along the boundaries of inclined columns clusters. Moreover, most of the observed thin microcracks were limited to either oxynitride top layer, TiAlCrSiN interlayer or TiAlCrN bond layer. Some larger macrocracks propagating between top layer and interlayer or between interlayer and bond layer were also observed in the central region of the scratch track, see Fig. 12b). However, these macrocracks exhibited reduced crack width in TiAlCrSiON top layer and TiAlCrN bond layer as compared to TiAlCrSiN interlayer, see Fig. 12d). This points towards promising potential of TiAlCrSiON top layer for an increased crack resistance compared to the TiAlCrSiN interlayer. The higher crack resistance of oxynitride top layer could presumably be attributed to beneficial combination of increased amorphous content, reduced hardness and higher ductility of the coating. However, further investigations with consideration of coating residual stress state are required for a comprehensive understanding on crack resistance of TiAlCrSiON coatings. The TiAlCrSiON surface in central region of the scratch track appeared flatter with no visible columnar morphology as compared to the coating surface on scratch shoulder region, see Fig. 12a) and b). This could be attributed to the downwards pressing of the columns by the indenter. This may result in inter-columnar or inter-column cluster shear sliding resulting in initiation of micro- and macrocracks, as observed in Fig. 12b) and d). In present investigations, no evidence of crack propagation between coating and cemented carbide substrate was found. This highlights the protective role of investigated coatings to bear bulk of the loading in application and delay the damage initiation and propagation in substrate for an increased the service of coated tools.

4. Conclusion

The cracking behavior of uncoated cemented carbide and coated compounds with thin and thick monolayer TiAlCrSiN and bilayer TiAlCrSiON/TiAlCrSiN coatings was studied under quasi-static and sliding normal loading conditions. Based on the presented results, following are the main conclusions.

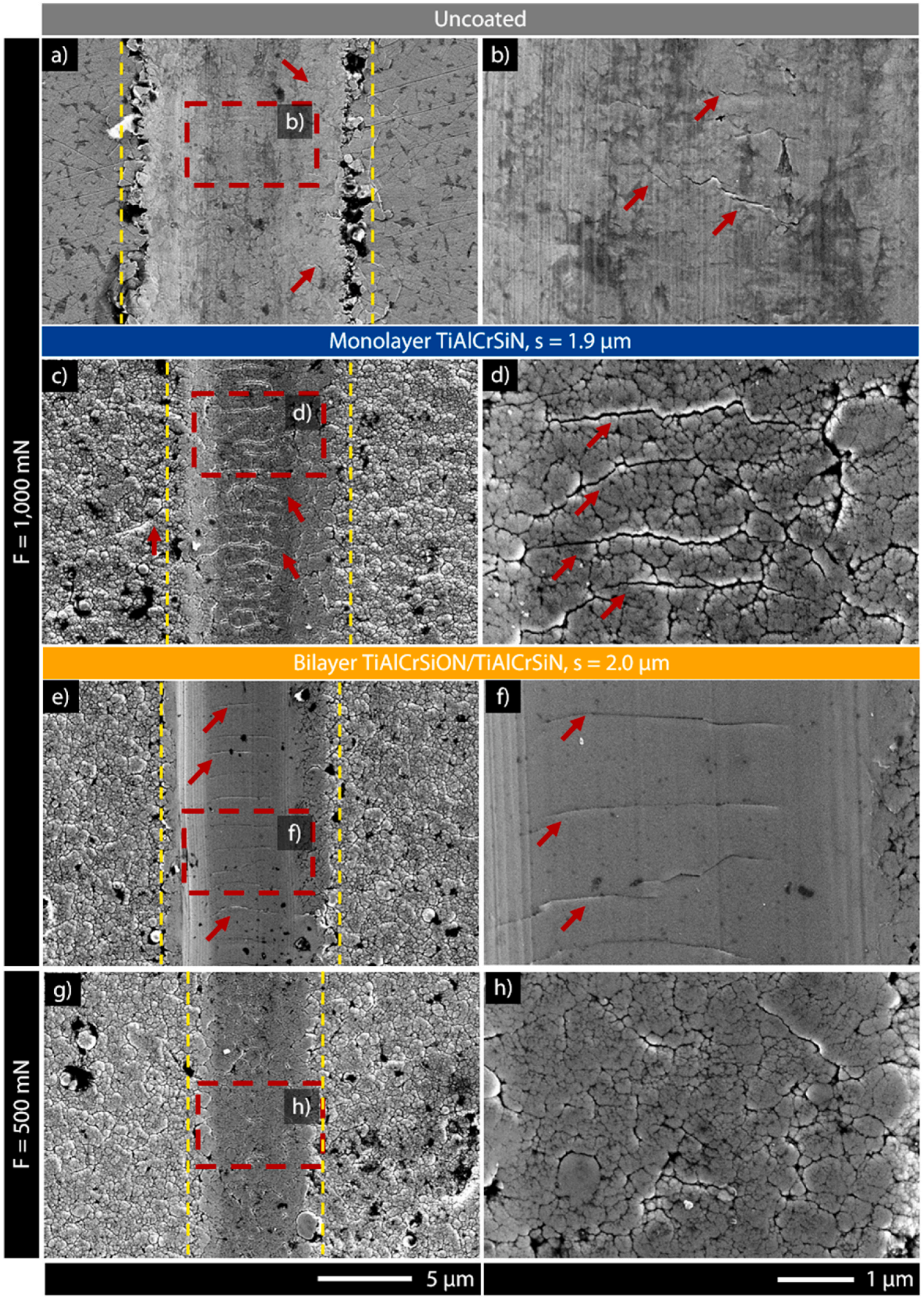

Fig. 8. Scratch tracks and surface cracks for (a–b) uncoated cemented carbide and (c–f) coated compounds with thin monolayer TiAlCrSiN and thin bilayer TiAlCrSiON/TiAlCrSiN.

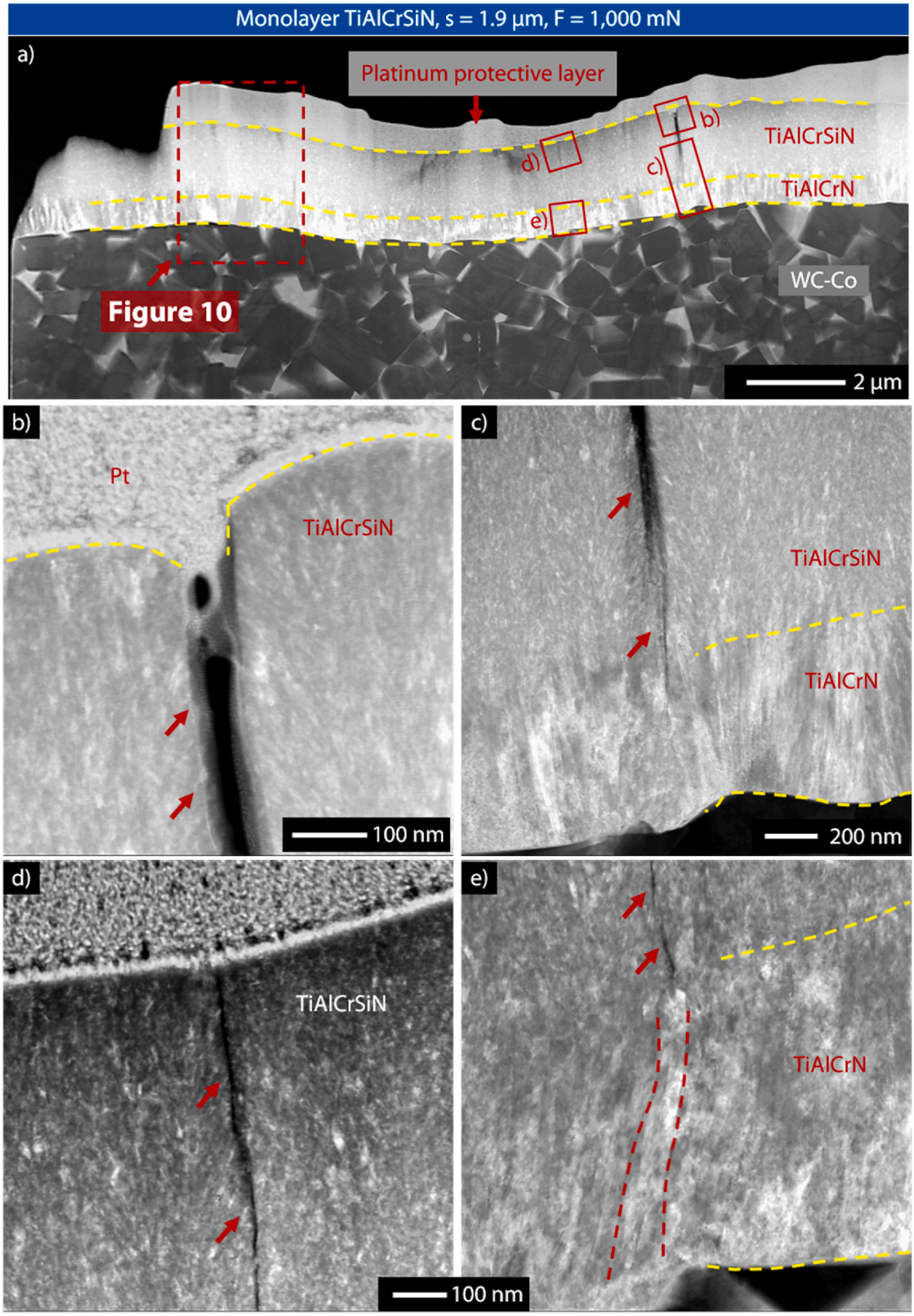

Fig. 9. STEM dark field (DF) images of (a) cross sectionally cut FIB lamella and (b–e) observed cracks in coating from F = 1000 mN scratch at coated compound with thin monolayer TiAlCrSiN.

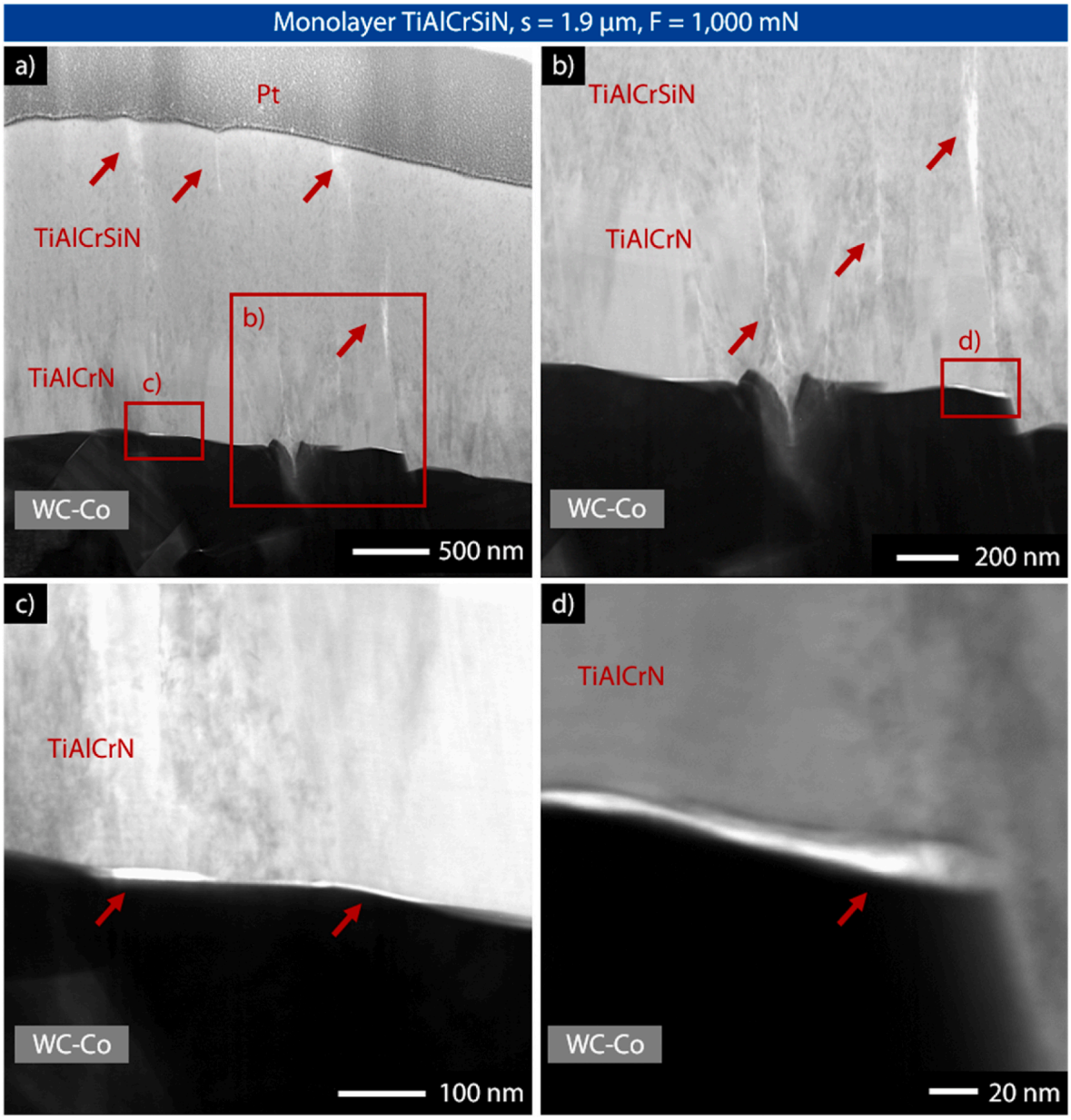

Fig. 10. STEM BF cross-section images from F = 1000 mN scratch shoulder region, marked in Fig. 9a), for coated compound with thin monolayer TiAlCrSiN.

- For TiAlCrSiN nanocomposite coatings on cemented carbide substrates, an increase in coating thickness may improve the overall crack resistance of the coated compounds under static and sliding normal loads. A higher coating thickness improved the load bearing capacity and reduced the overall permanent deformation of the coated compound.
- For quasi-static normal loading, plastic work percentage η_{plast}, calculated from nanoindentation force-displacement curves, appears to be an important indicator for resistance of coated compounds against surface cracks. In present study, $\eta_{plast} \leq 53$ % was recognized as the criterion for prevention of surface cracks in the investigated compounds.
- The bilayer TiAlCrSiON/TiAlCrSiN architecture exhibited a promising potential to improve the crack resistance of the coated compound.
- Under sliding normal load, the cracks in coating cross-section mainly propagate along column or column cluster boundaries. Around scratch shoulder region, the cracks originate as the columnar coating deforms through column inclination and inter-columnar sliding. In central region of the scratch track, the coating columns are pushed downwards by the indenter and the cracks may appear due to shear sliding between columns or column clusters. This contributes to material bulging on scratch shoulders. Here, depending on the coating architecture and chemical composition, the interface between individual layers, for instance between top layer and bond layer in present case, may act as an additional barrier to crack propagation. Moreover, the improved loading bearing capacity of the coating with higher thickness may reduce the overall permanent coating and substrate deformation, minimize the material bulging on scratch shoulders and improve the crack resistance of the coated compound.

CRediT authorship contribution statement

K. Bobzin: Funding acquisition, Conceptualization, Project administration, Resources, Supervision, Writing – review & editing. **C. Kalscheuer:** Conceptualization, Funding acquisition, Project administration, Supervision, Writing – review & editing. **M. Tayyab:**

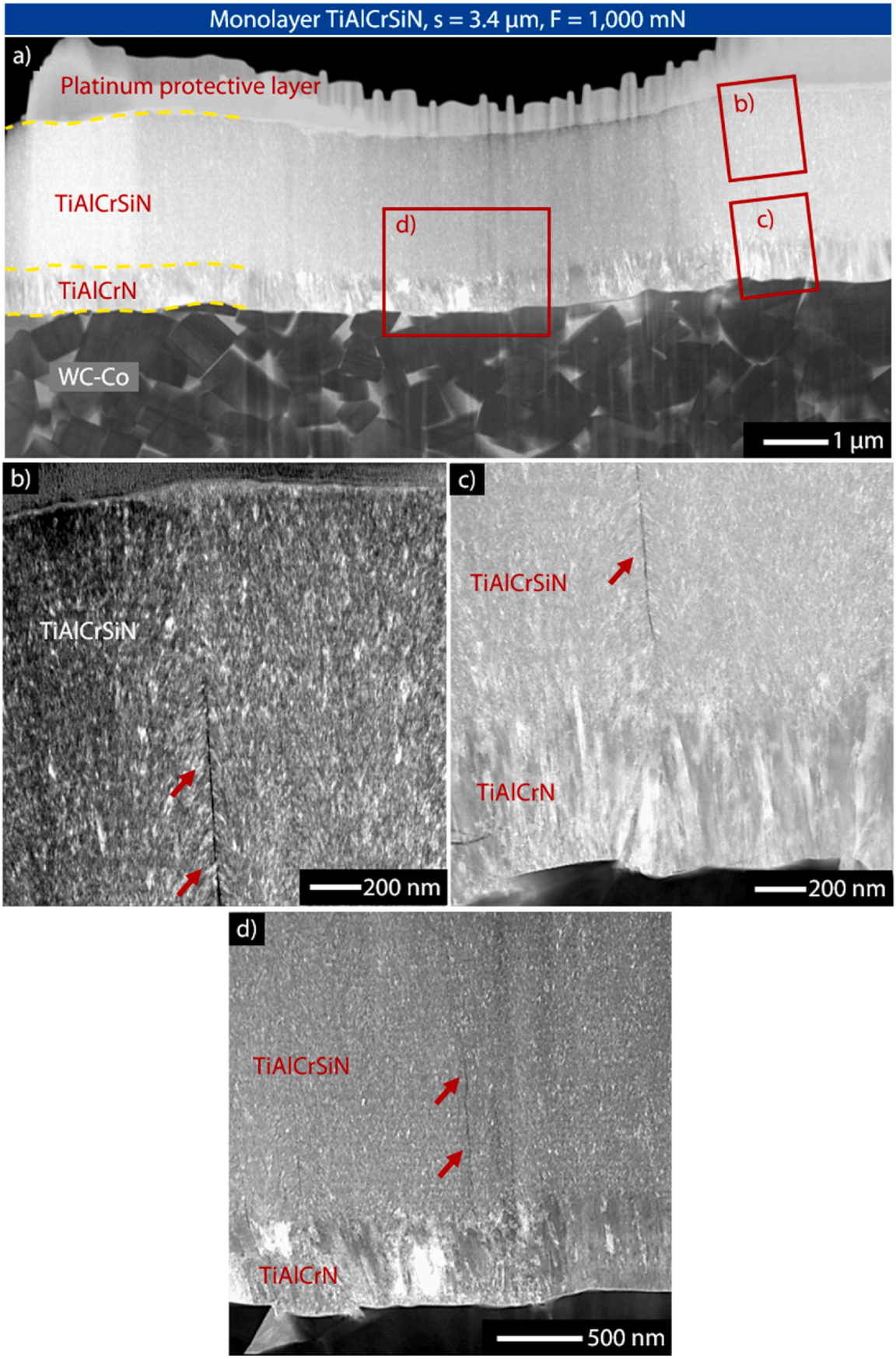

Fig. 11. STEM DF images of (a) cross sectionally cut FIB lamella and (b–d) observed cracks in coating from F = 1000 mN scratch at coated compound with thick monolayer TiAlCrSiN.

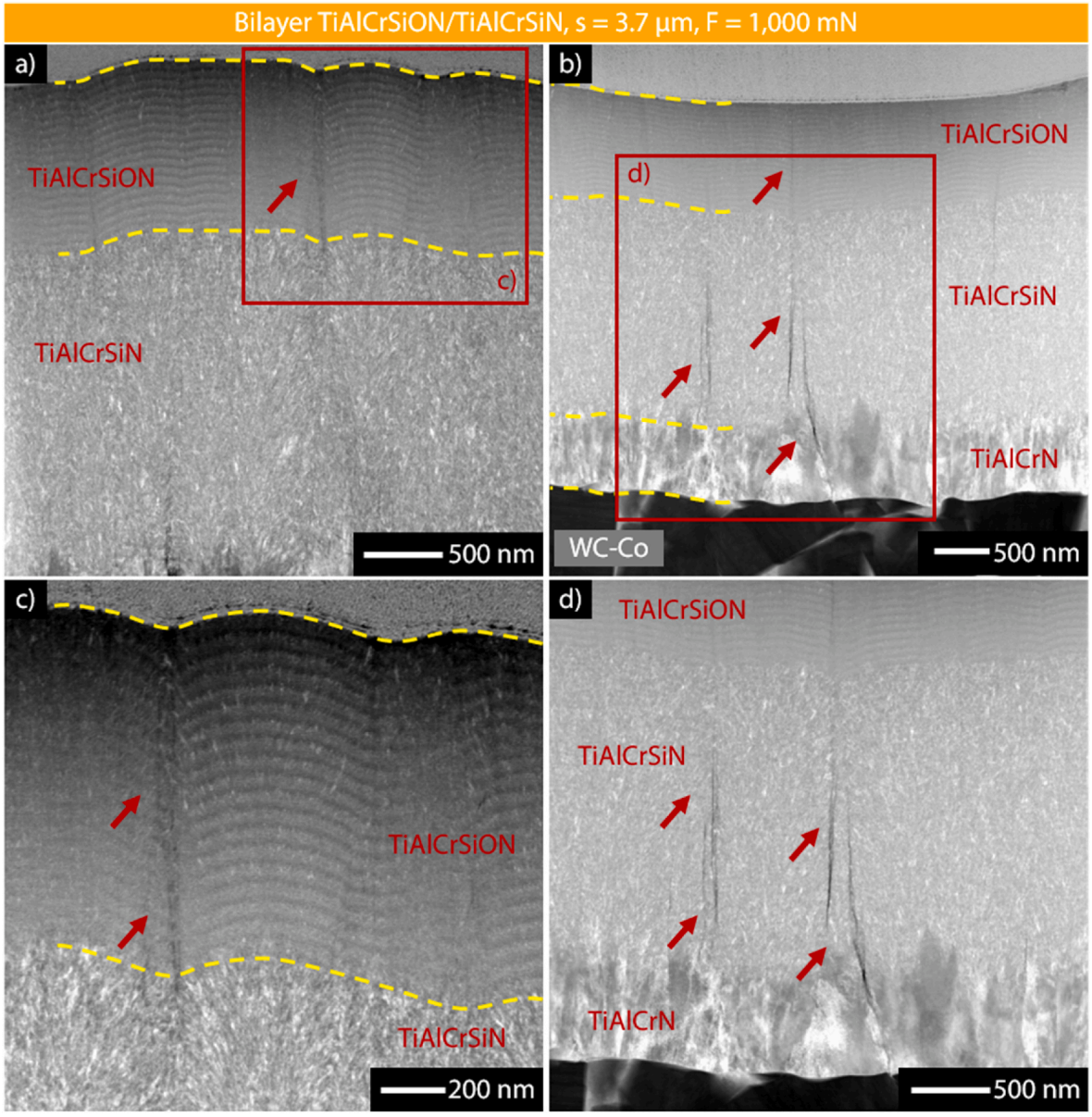

Fig. 12. STEM DF cross-section images from F = 1000 mN scratch (a&c) shoulder region and (b&d) central region for coated compound with thick bilayer TiAlCrSiON/TiAlCrSiN.

Conceptualization, Formal analysis, Investigation, Methodology, Visualization, Writing – original draft.

Declaration of competing interest

The authors declare that they have no known competing financial interests or personal relationships that could have appeared to influence the work reported in this paper.

Acknowledgement

The authors gratefully acknowledge the financial support of the German Research Foundation, Deutsche Forschungsgemeinschaft (DFG), within the project 521280523, BO 1979/99-1

References

[1] S. Vepřek, S. Reiprich, L. Shizhi, Superhard nanocrystalline composite materials: the TiN/Si3N4 system, Appl. Phys. Lett. 66 (1995) 2640–2642, https://doi.org/10.1063/1.113110.

[2] N. Jiang, Y. Shen, Y.-W. Mai, T. Chan, S.C. Tung, Nanocomposite Ti–Si–N films deposited by reactive unbalanced magnetron sputtering at room temperature, Mater. Sci. Eng., B 106 (2004) 163–171, https://doi.org/10.1016/j.mseb.2003.09.033.

[3] E. Huber, S. Hofmann, Oxidation behaviour of chromium-based nitride coatings, Surf. Coating. Technol. 68–69 (1994) 64–69, https://doi.org/10.1016/0257-8972(94)90139-2.

[4] K. Bobzin, T. Brögelmann, H.J. Maier, T. Heidenblut, C. Kahra, M. Carlet, Influence of residual stresses in hard tool coatings on the cutting performance, J. Manuf. Process. 69 (2021) 340–350, https://doi.org/10.1016/j.jmapro.2021.08.011.

[5] K. Bobzin, T. Brögelmann, N.C. Kruppe, M. Carlet, Investigation on the incorporation of oxygen and thermal stability of HPPMS TiAlCrSiON nanolayer coatings, Surf. Coating. Technol. 418 (2021) 127231, https://doi.org/10.1016/j.surfcoat.2021.127231.

[6] K. Bobzin, C. Kalscheuer, M. Tayyab, Tribological behavior of TiAlCrSiN coated cutting tools, Vak Forsch Prax 36 (2024) 18–22, https://doi.org/10.1002/vipr.202400817.

[7] K. Bobzin, T. Brögelmann, N.C. Kruppe, M. Carlet, Wear behavior and thermal stability of HPPMS (Al,Ti,Cr,Si)ON, (Al,Ti,Cr,Si)N and (Ti,Al,Cr,Si)N coatings for

cutting tools, Surf. Coating. Technol. 385 (2020) 125370, https://doi.org/10.1016/j.surfcoat.2020.125370.

[8] A. Inspektor, P.A. Salvador, Architecture of PVD coatings for metalcutting applications: a review, Surf. Coating. Technol. 257 (2014) 138–153, https://doi.org/10.1016/j.surfcoat.2014.08.068.

[9] J. Jian, J.H. Lee, Y. Liu, F. Khatkhatay, K. Yu, Q. Su, X. Zhang, L. Jiao, H. Wang, Plastic deformation in nanocrystalline TiN at ultra-low stress: an in situ nanoindentation study, Materials Science and Engineering: A 650 (2016) 445–453, https://doi.org/10.1016/j.msea.2015.10.002.

[10] K. Bobzin, T. Brögelmann, N.C. Kruppe, M. Arghavani, J. Mayer, T.E. Weirich, On the plastic deformation of chromium-based nitride hard coatings deposited by hybrid dcMS/HPPMS: a fundamental study using nanoscratch test, Surf. Coating. Technol. 308 (2016) 298–306, https://doi.org/10.1016/j.surfcoat.2016.05.093.

[11] P. Wieciński, J. Smolik, H. Garbacz, K.J. Kurzydłowski, Failure and deformation mechanisms during indentation in nanostructured Cr/CrN multilayer coatings, Surf. Coating. Technol. 240 (2014) 23–31, https://doi.org/10.1016/j.surfcoat.2013.12.006.

[12] J. Shuai, X. Zuo, Z. Wang, P. Guo, B. Xu, J. Zhou, A. Wang, P. Ke, Comparative study on crack resistance of TiAlN monolithic and Ti/TiAlN multilayer coatings, Ceram. Int. 46 (2020) 6672–6681, https://doi.org/10.1016/j.ceramint.2019.11.155.

[13] P. Panjan, A. Miletić, A. Drnovšek, P. Terek, M. Čekada, L. Kovačević, M. Panjan, Cracking resistance of selected PVD hard coatings, Coatings 14 (2024) 1452, https://doi.org/10.3390/coatings14111452.

[14] K. Bobzin, C. Kalscheuer, M. Tayyab, Effect of CrAlN coating properties on impact fatigue of tool steel, Surf. Coating. Technol. 471 (2023) 129869, https://doi.org/10.1016/j.surfcoat.2023.129869.

[15] A.A. Vereschaka, S.N. Grigoriev, Study of cracking mechanisms in multi-layered composite nano-structured coatings, Wear 378–379 (2017) 43–57, https://doi.org/10.1016/j.wear.2017.01.101.

[16] A.A. Vereschaka, S.N. Grigoriev, N.N. Sitnikov, A.D. Batako, Delamination and longitudinal cracking in multi-layered composite nano-structured coatings and their influence on cutting tool life, Wear 390–391 (2017) 209–219, https://doi.org/10.1016/j.wear.2017.07.021.

[17] W.C. Oliver, G.M. Pharr, An improved technique for determining hardness and elastic modulus using load and displacement sensing indentation experiments, J. Mater. Res. 7 (1992) 1564–1583, https://doi.org/10.1557/JMR.1992.1564.

[18] E. Török, A.J. Perry, L. Chollet, W.D. Sproul, Young's modulus of TiN, TiC, ZrN and HfN, Thin Solid Films 153 (1987) 37–43, https://doi.org/10.1016/0040-6090(87)90167-2.

[19] J. Chen, S.J. Bull, On the factors affecting the critical indenter penetration for measurement of coating hardness, Vacuum 83 (2009) 911–920, https://doi.org/10.1016/j.vacuum.2008.11.007.

[20] M. Arghavani, Elastic-Plastic Deformation and Cracking Behavior of Thin Hard Chromium-Based Coatings. Dissertation. ISBN: 978-3-8440-6625-8.